Scripta Materialia 147 (2018) 1–5

Contents lists available at ScienceDirect

Scripta Materialia

journal homepage: www.elsevier.com/locate/scriptamat

Regular article

# Cracking behavior of helium-irradiated small-volume copper

Wei-Zhong Han *, Ming-Shuai Ding, Zhi-Wei Shan

*Center for Advancing Materials Performance from the Nanoscale (CAMP-Nano) & Hysitron Applied Research Center in China (HARCC), State Key Laboratory for Mechanical Behavior of Materials, Xi'an Jiaotong University, Xi'an, 710049, China*

ARTICLE INFO

*Article history:*
Received 4 September 2017
Received in revised form 5 December 2017
Accepted 24 December 2017
Available online xxxx

*Keywords:*
Helium bubble
Cracking
Irradiation
Cavity
Nano-bridge

ABSTRACT

Radiation-induced grain-boundary helium bubbles are the cause of the significant helium embrittlement. However, the influence of grain-interior helium bubbles on the cracking behavior of metals has not been explored. Here, we investigate the cracking propensity of helium-irradiated small-volume Cu single-crystals, and compare with those of Cu single-crystals and Cu bicrystals. We found that the irradiation-induced helium bubbles only slightly increased the cracking propensity of the single-crystal Cu, while the cracking resistance of the helium-irradiated Cu single-crystals was superior to that of the Cu bicrystals, both with and without helium bubbles.



Radiation damage plays a decisive role in determining the lifetime of the key structural materials of both fission and fusion reactors [1–4]. Neutron bombardment not only produces a large number of radiation defects, but also causes nuclear reactions, which may generates considerable concentrations of foreign elements within the metals [1–4]. In particular, the inert gas helium, which is the product of (n, α) reactions, has an adverse effect on the mechanical properties of metals, even in low concentrations [5–9].

The detrimental effect of helium on the properties of materials has a significant connection with the formation of helium bubbles [1–9]. Owing to its extremely low solubility in metals, helium co-precipitates with radiation-induced vacancies to form nanobubbles almost immediately following its formation; this occurs via a nuclear reaction or ion implantation [10,11]. One significantly harmful effect caused by helium is high-temperature embrittlement. In general, high-temperature ductility losses observed during tensile, creep, and fatigue tests are owing to the presence of helium bubbles at grain boundaries (GB) [1–9]. At high temperatures, these GB bubbles grow explosively under the promotion of stress, and lead to intergranular fracture. This GB rupture occurs owing to the enhanced initiation and/or growth of GB cracks due to GB helium-bubble growth and coalescence [1,9].

In general, the roles of GB helium bubbles and matrix bubbles differ, and should be studied separately. GB helium bubbles are usually larger than matrix bubbles because of differences in the sink strength of GBs and grain interiors [1,7]. Larger GB helium bubbles tend to initiate GB cracks and cause premature brittle failure under stress [1–9]. In contrast, grain-interior bubbles function as internal dislocation sources and shearable precipitates, which are beneficial for the homogeneous and stable plastic deformation of small-volume metals [12–18]. However, owing to the premature intergranular failure of metals induced by GB helium bubbles, the effect of grain-interior helium bubbles on crack nucleation and propagation has not been fully explored. In this study, we explore the cracking behavior of small-volume single-crystal Cu with a high density of helium nanobubbles, and compare its crack behavior with those of Cu single-crystals and Cu bi-crystals, both with and without helium irradiation.

The Cu samples with helium bubbles were prepared by performing helium implantation (200 keV ions) on well-annealed Cu at 450 °C, with a fluence of $2 \times 10^{17}$ ions $cm^{-2}$ [19]. The current implantation conditions were designed to forming high density of helium bubbles in the model materials of Cu and did not relevant to a real nuclear environment. Numerous helium bubbles with average size of 6.6 nm were precipitated inside the grains, and slightly larger helium bubbles (>10 nm) were formed along the GBs [16–19]. These bubbles are expected to be under near equilibrium conditions because of the slow cooling conditions that followed high-temperature implantation. The radiation damage (displacements per atom, DPA) and helium concentration of each Cu sample were estimated using Monte Carlo simulations, the details of which are found elsewhere [13,19]. All the notched cantilever samples intended for the in situ cracking tests were machined, from the region of the material (between 440 nm and 760 nm from the top surface of implantation) with the helium concentration varying from 3 to 8 at.% (more details can be found in [16,18]), using the focused ion beam (FIB) technique. The density of helium bubbles is roughly the same across the whole cantilever sample. The notched cantilever samples had a fixed geometry and dimensions, as shown in Fig. 1a. All cantilever samples had a thickness of 50 nm. The initial opening angle of the cantilever

* Corresponding author.
*E-mail address:* wzhanxjtu@mail.xjtu.edu.cn (W.-Z. Han).

https://doi.org/10.1016/j.scriptamat.2017.12.029
1359-6462/

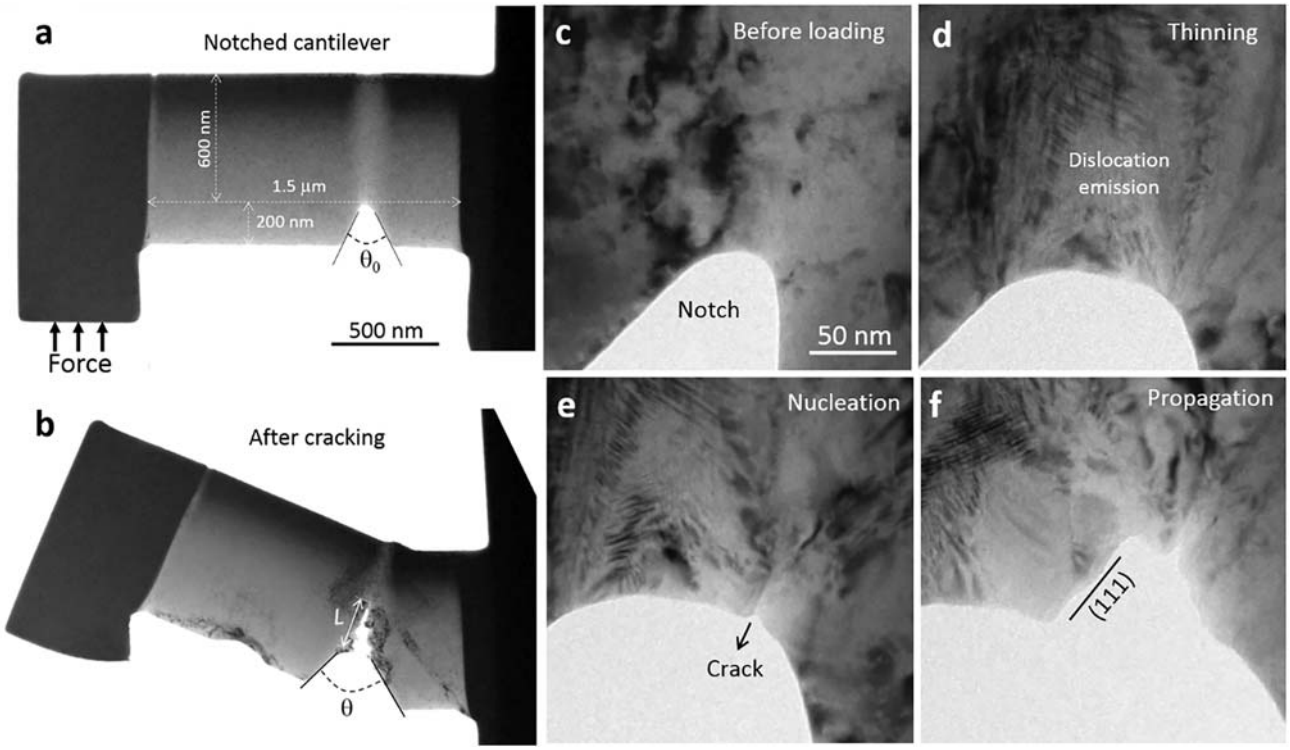


**Fig. 1.** Measurement of the crack propensity of a small-volume Cu single-crystal, with a compressive direction of [311]. (a) The geometry of the notched small-volume Cu cantilever used for the cracking test. (b) The deformed small-volume Cu cantilever with an increased opening angle, and crack at the front of the notch. (c) The initial microstructure of the notch. (d) Dislocation emission and thinning of the sample at the front of the notch, upon loading. (e) Crack beginning to nucleate at the groove formed on the edge of the notch, due to dislocation emission. (f) Crack propagation under further loading, and crack surface forming along the (111) plane.

samples was designed to have a constant value of $\theta_0 \equiv 40^\circ \pm 2^\circ$, as displayed in Fig. 1a. Following apply a force on the left side of the notched cantilever samples, the final opening angles were increased, and had final values of $\theta = 60^\circ - 69^\circ$, as demonstrated in Fig. 1b. Upon loading, cracks were formed at the front of the notches in the majority of the tested samples; the length of each crack is denoted as $L$, as marked in Fig. 1b. A parameter was used to determine the cracking propensity of the cantilever samples. It is defined as the ratio between the cracking length ($L$) and the net increase in the opening angle, $C_{propensity} = \frac{L}{\theta - \theta_0}$; this parameter was used to qualitatively compare the cracking behaviors of the various types of small-volume Cu samples. All in situ mechanical tests were performed using a PicoIndentor (PI95) located inside a transmission electron microscope (200 kV), with a loading rate of 5 nm/s. Four types of samples were investigated, namely a fully dense Cu (FD-Cu) single-crystal; a Cu single-crystal with helium nanobubbles (NB-Cu); a Cu bicrystal with a high-angle GB (FD-Cu bicrystal); and a Cu bicrystal with a helium bubble-damaged GB (NB-Cu bi-crystal). More than 20 in situ cantilever tests were performed to explore the influence of the helium bubbles on the cracking behavior of the small-volume Cu samples.

Fig. 1c to f shows images which display the cracking behavior of a typical FD-Cu single-crystal cantilever sample, with loading along the [311] direction. The notched area of the sample appears clean with few linear dislocations, with the exception of some surface damage that was generated during the FIB machining. Upon loading, the notch opening angle increases gradually, and is accompanied by the profuse emission of dislocations from the notch tip, as indicated by the U-shape contrast contours located at the front of the notch, shown in Fig. 1d and Movie S1. The sample becomes increasingly thinner with the emission of dislocations, and a groove-like feature develops gradually, indicating the transition from homogeneous deformation to strain localization, as shown in Fig. 1e and Movie S1. The groove feature that formed at the edge of the notch of the FD-Cu single-crystal represents the precursor for crack nucleation. Upon further loading, the groove gradually transforms into an edge crack (Fig. 1e). Subsequently, with further deformation, the crack propagates along the groove, and forms a fracture surface that is close to the (111) plane. The plastic deformation during cracking is mainly confined around the crack tip area, as shown in Fig. 1 and Movie S1. Based on the results of the multiple cracking tests performed, the cracking behavior of the FD-Cu single-crystals could be categorized by three steps: dislocation emission with sample thinning, strain localization with groove development, and crack nucleation at the groove and further propagation under loading.

Fig. 2 displays the cracking behavior of a typical NB-Cu single-crystal cantilever sample, with a high density of helium nanobubbles; the sample is loaded along the [100] direction. The helium nanobubbles are distributed homogeneously and have an average size of $<d> = 6.6$ nm, as shown in Fig. 2a. The edge of the notch has a small bubble-free zone, which is probably owing to the sharp reduction in the thickness of the marginal region [18]. Upon loading, partial dislocations begin to activate at the front of the notch, forming numerous stacking faults (SFs) that cut through the helium nanobubbles [14,16], as shown in Fig. 2b and Movie S2. Simultaneously, the mechanical loading induces tear deformation at the notch front, which partially promotes an increase in the notch length (Movie S2). With further deformation, a number of helium nanobubbles at the notch tip begin to grow by absorbing the deformation-induced vacancies [1,14]. Subsequently, some of the helium bubbles, located along the sample-thickness direction, begin to coalesce and form cavities/holes within the samples, as shown in Fig. 2b and c, and Movie S2. The sizes of these perforations further increases as the loading continues, and the spacing between gradually decreases. This finally leads to the link-up of multiple cavities, as shown in Fig. 2d and e, and Movie S2. This is a critical step with regard to the formation of internal cracks within the NB-Cu single crystal. During the growth and propagation of the internal cracks in the NB-Cu single-crystal sample, numerous nano-bridges develop through the elongation of the nano-

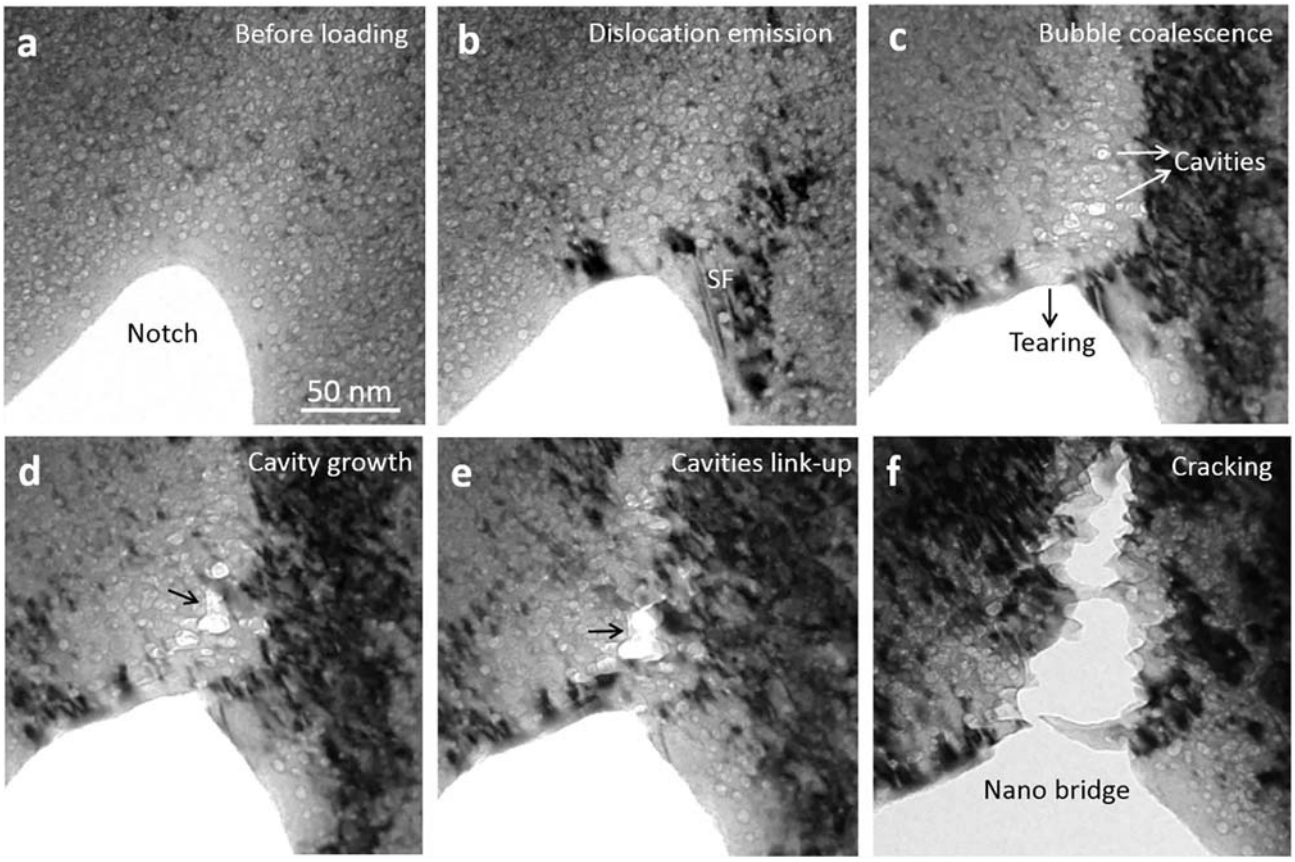


**Fig. 2.** Images of the cracking behavior of a NB-Cu single-crystal cantilever with a high density of helium bubbles, with a compressive direction of [100]. (a) The microstructure of the helium bubbles at the front of the notch prior to loading. (b) Partial dislocation emissions, leading to the formation of stacking faults (SFs) at the notched area. (c) Coalescence of helium bubbles along the sample-thickness direction, triggering the formation of large holes/cavities. (d) Further in-plane bubble coalescence, promoting the growth of cavities. (e) Crack nucleation via the link-up of isolated cavities; (f) Nano-bridge formation during crack propagation.

walls that separate the helium nanobubbles, as shown in Fig. 2f and Movie S2. During cracking, the bridging is able to delay the failure of the NB-Cu samples [20]. Further cracking tests were performed on the NB-Cu single-crystal, which demonstrated similar cracking behavior. According to the results of these experimental investigations, the cracking of the NB-Cu single crystal could be summarized by four steps: dislocation emission with tearing, bubble growth and coalescence along the sample thickness, crack nucleation via cavity growth and link-up, and crack propagation with nano-bridging.

To explore the differences between the cracking behaviors of the Cu single-crystals and bicrystals, we performed further tests on the samples with high-angle GBs, both with and without helium bubbles. Fig. 3a to c shows the cracking processes associated with the FD-Cu bicrystal that has a high-angle GB located along the notch direction. The GB is marked by a dashed line, as shown in Fig. 3a. Upon loading, a crack with a length of almost 50 nm immediately nucleates at the intersection point of the notch and GB. Subsequently, the crack directly propagates along the GB; this is accompanied by dislocation emission, as shown in Fig. 3c and Movie S3. Fig. 3d to f displays the cracking behavior of the NB-Cu bicrystal with a high-angle GB along the vertical direction of the notch. Many helium bubbles with sizes larger than 15 nm decorate the GB, as shown in Fig. 3d. Similar to the behavior observed for the FD-Cu bicrystal, a crack rapidly nucleates at the intersection point of the notch and GB, despite the GB's location being in an unfavorable direction for cracking, as shown in Fig. 3e and Movie S4. Notably, at the point of crack nucleation at the edge, significant GB cleavage, due to the connection of the GB helium bubbles, occurs immediately; feature that resembles a tooth crack forms along the two edges of the helium-damaged GB, as displayed in Fig. 3f and Movie S4. Crack nucleation and propagation occur almost simultaneously in the case of the NB-Cu bicrystal. This is indicative of the adverse influence of GB helium bubbles on the premature failure of metals [1–9]. Almost no dislocation emission and nano-bridges are observed during the crack propagation of the NB-Cu bicrystal; this significantly differs from the results of the observations of the NB-Cu and FD-Cu single crystals.

Fig. 4 shows a qualitative comparison of the cracking propensity of the aforementioned four types of Cu cantilever samples. The FD-Cu single crystal samples with various orientations exhibit cracking rates of $0-5$ nm/degree; the lowest among the four types of samples. The NB-Cu single crystal samples with various orientations exhibit cracking rates of $2-10$ nm/degree (Fig. 4); this indicates that the high density of irradiation-induced helium nanobubbles only slightly increases the cracking propensity of the Cu single-crystals. The minimal difference in the cracking propensity of NB-Cu and FD-Cu single crystals is due to the forming of nanobridges in NB-Cu, which is a unique toughening mechanism to enhance the crack resistance. However, the FD-Cu bicrystal has a much greater cracking propensity than those of the Cu single-crystals. In the case of the FD-Cu bicrystal with a high-angle GB along the notch direction, the measured crack rate is approximately 12 nm/degree; this is almost twice that of the FD-Cu. Notably, the NB-Cu bicrystal with a helium-bubble damaged high-angle GB displays a considerably faster cracking rate, ~17 nm/degree, which is almost twice that of the NB-Cu single-crystal. In this study, due to the difficult of cutting small-volume bicrystal samples with well-aligned GB from a polycrystalline Cu thin foil, we only tested two bicrystal cracking samples. When comparing the fracture behavior of bicrystal Cu with that of the FD-Cu and the NB-Cu single-crystals, a trend is identified, as shown in Fig. 4. It is clear that irradiation-induced helium bubbles could only slightly increase the cracking propensity of the Cu single-crystal, while the NB-Cu single-crystal demonstrates superior cracking

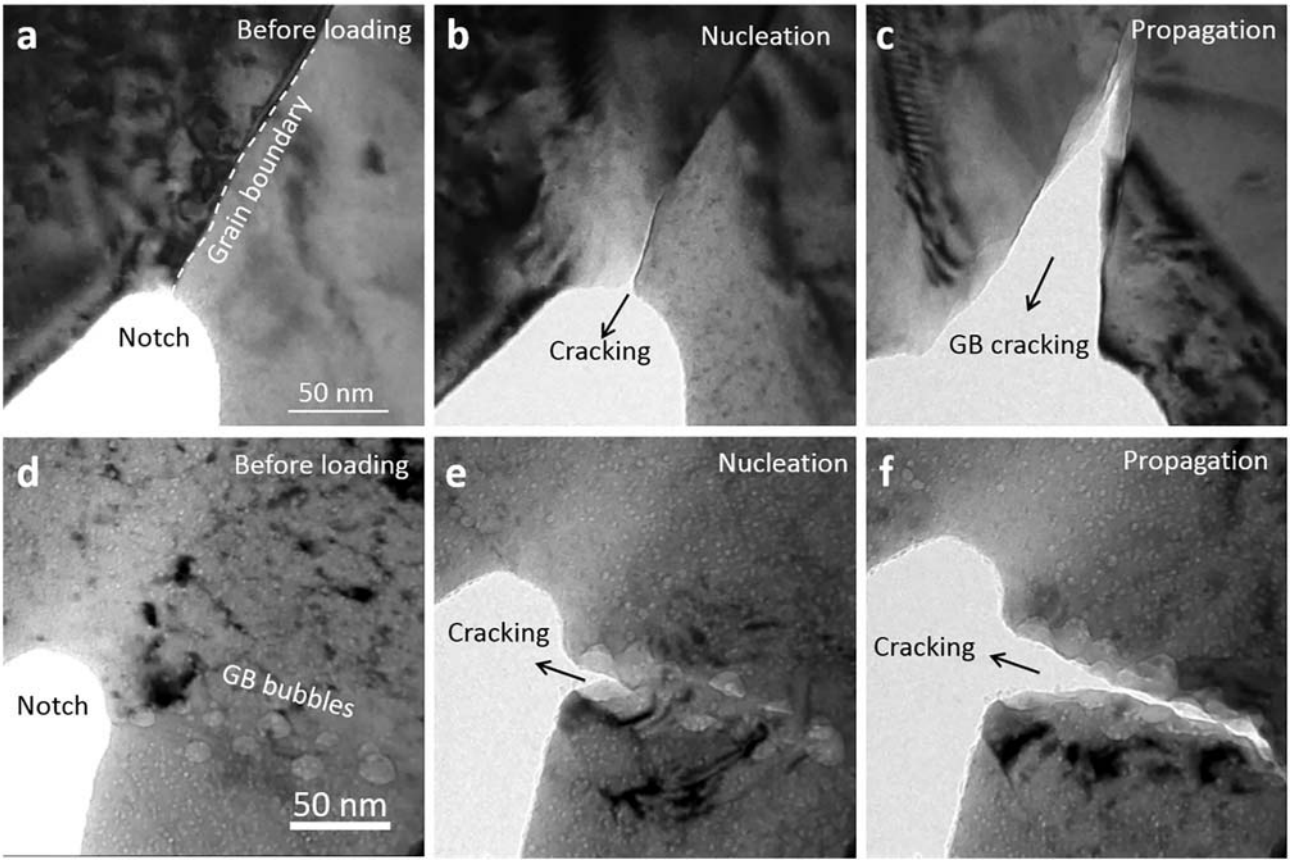


**Fig. 3.** Typical examples of cracking along the grain boundaries of FD-Cu and NB-Cu bicrystals. (a)–(c) Cracking along a high-angle GB of a FD-Cu bicrystal. (d)–(f) Cracking along a helium bubble-damaged high-angle GB of a NB-Cu bicrystal.

resistance to those of the FD-Cu and NB-Cu bicrystals. The NB-Cu bicrystal demonstrates the highest cracking rate among the four types of small-volume samples explored; this is indicative of the significant adverse influence of the GB helium bubbles on the mechanical performance of metals and alloys [1–8].

In summary, we investigated the cracking behavior of small-volume Cu samples with a high density of irradiation-induced helium bubbles, and compared their cracking propensities with those of single-crystal Cu and Cu bicrystals, both with and without helium irradiation. We observed that the radiation-induced helium bubbles could only slightly increase the cracking propensity of the single-crystal Cu. However, the cracking resistance of the NB-Cu single-crystal was determined to be superior to those of the FD-Cu and NB-Cu bicrystals because of the formation of nano-bridges during crack propagation.

Supplementary data to this article can be found online at https://doi.org/10.1016/j.scriptamat.2017.12.029.

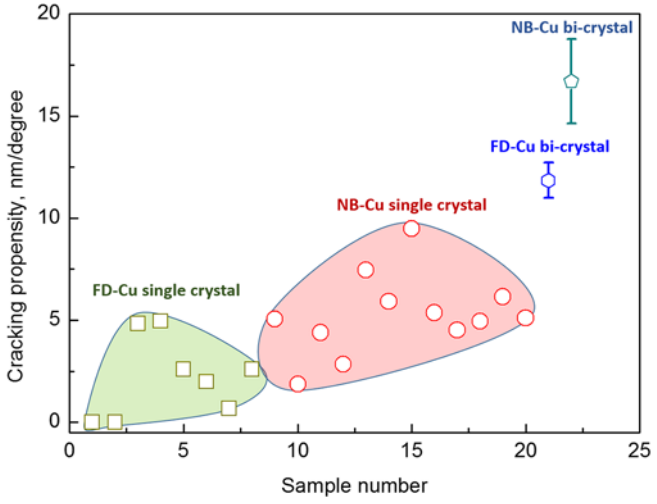


**Fig. 4.** Comparison of the cracking propensity of FD-Cu single-crystals, NB-Cu single-crystals, FD-Cu bicrystals, and NB-Cu bicrystals.

## Acknowledgements

This work was supported by the National Key Research and Development Program of China (2017YFB0702301) and the National Natural Science Foundation of China (Grant Nos. 51471128, 51621063). W.Z.H. would like to thank the support of Youth Thousand Talents Program of China and the Young Talent Support Plan of XJTU. We appreciate the assistance of E.G.F and Y.Q.W in ion implantation.

## References

[1] H. Ullmaier, Nucl. Fusion 8 (1984) 1039.
[2] G.R. Odette, M.J. Alinger, B.D. Wirth, Annu. Rev. Mater. Res. 38 (2008) 471.
[3] S.J. Zinkle, G.S. Was, Acta Mater. 61 (2013) 735.
[4] Y. Ueda, K. Schmid, M. Balden, J.W. Coenen, Th. Loewenhoff, A. Lto, A. Hasegawa, C. Hardie, M. Porton, M. Gilbert, Nucl. Fusion 57 (2017), 092006.
[5] A.N. Hughes, J.R. Caley, J. Nucl. Mater. 10 (1963) 60.
[6] G.E. Lucas, J. Nucl. Mater. 206 (1993) 287.
[7] H. Trinkaus, B.N. Singh, J. Nucl. Mater. 323 (2003) 229.
[8] M.R. Gilbert, S.L. Dudarev, D. Nguyen-Manh, S. Zheng, L.W. Packer, J.C. Sublet, J. Nucl. Mater. 442 (2013) S755.
[9] E. Martinez, B.P. Uberuaga, B.D. Wirth, Nucl. Fusion 57 (2017), 086044.
[10] K. Farrell, Radiat. Eff. 53 (1980) 175.
[11] C.C. Fu, F. Willaime, Phys. Rev. B 72 (2005), 064117.
[12] N. Li, N.A. Mara, Y.Q. Wang, M. Nastasi, A. Misra, Scr. Mater. 64 (2011) 974.
[13] Q. Guo, J.R. Greer, Scr. Mater. 66 (2012) 272.

[14] M.S. Ding, J.P. Du, L. Wan, S. Ogata, L. Tian, E. Ma, W.Z. Han, J. Li, Z.W. Shan, Nano Lett. 16 (2016) 4118.
[15] A. Reichardt, M. Ionescu, J. Davis, L. Edwards, R.P. Harrison, P. Hosemann, D. Bhattacharyya, D. Bhattacharyya, Acta Mater. 100 (2015) 147.
[16] M.S. Ding, L. Tian, W.Z. Han, J. Li, E. Ma, Z.W. Shan, Phys. Rev. Lett. 117 (2016) 215501.
[17] W.Z. Han, J. Zhang, M.S. Ding, L. Lv, W.H. Wang, G.H. Wu, Z.W. Shan, J. Li, Nano Lett. 17 (2017) 3725.
[18] W.Z. Han, M.S. Ding, R.L. Narayana, Z.W. Shan, Adv. Eng. Mater (2017)https://doi.org/10.1002/adem.201700357.
[19] W.Z. Han, M.J. Demkowicz, E.G. Fu, Y.Q. Wang, A. Misra, Acta Mater. 60 (2012) 6341.
[20] A. Pineau, A.A. Benzerga, T. Pardoen, Acta Mater. 107 (2016) 424.